MATEMATIKA, 2018, Special Issue, 189–201

Heat and Mass Transfer of Magnetohydrodynamics (MHD) Boundary Layer Flow using Homotopy Analysis Method

Nur Liyana Nazari, Ahmad Sukri Abd Aziz, Vincent Daniel David* **and Zaileha Md Ali**

Faculty of Computer and Mathematical Sciences
Universiti Teknologi MARA, Shah Alam, Selangor

*Corresponding author: vincent@tmsk.uitm.edu.my

Article history
Received: 13 September 2018
Received in revised form: 6 December 2018
Accepted: 17 December 2018
Published on line: 31 December 2018

Abstract Heat and mass transfer of MHD boundary-layer flow of a viscous incompressible fluid over an exponentially stretching sheet in the presence of radiation is investigated. The two-dimensional boundary-layer governing partial differential equations are transformed into a system of nonlinear ordinary differential equations by using similarity variables. The transformed equations of momentum, energy and concentration are solved by Homotopy Analysis Method (HAM). The validity of HAM solution is ensured by comparing the HAM solution with existing solutions. The influence of physical parameters such as magnetic parameter, Prandtl number, radiation parameter, and Schmidt number on velocity, temperature and concentration profiles are discussed. It is found that the increasing values of magnetic parameter reduces the dimensionless velocity field but enhances the dimensionless temperature and concentration field. The temperature distribution decreases with increasing values of Prandtl number. However, the temperature distribution increases when radiation parameter increases. The concentration boundary layer thickness decreases as a result of increase in Schmidt number.

Keywords Heat and mass transfer; MHD; stretching sheet; radiation; homotopy analysis method.

Mathematics Subject Classification 80A20 ;76W05; 58B05

1 Introduction

Heat and mass transfer play a huge role in industry and manufacturing processes such as the making of glass-fiber, cooling of electronic equipment, filtration, and atomic power plants [1]. Numerous studies have been conducted to analyze the effects of heat and mass transfer in boundary layer flow. Heat and mass transfer in magnetohydrodynamics flow over an exponentially stretching sheet in a thermally stratified medium was investigated by [2]. Mori *et al.* [3] analyze the effects of convective heat and mass transfer under the laminar flow past a flat plate of finite thickness. The study of the characteristics of heat and mass transfer in a viscoelastic boundary layer flow over an exponentially stretching sheet has been conducted by Sanjayanand

and Khan [4]. Serna [5] examined the nanofluid boundary layers with heat and mass transfer properties.

Boundary layer flow on stretching sheet has applications in industry and technology processes. For instance, polymer extrusion in melt spinning process, annealing and tinning of copper wires, and production of metallic sheets. In these processes, the rate of heat transfer from the structure of boundary layer past a sheet influences the property of the desired product. Authors that studied flow over a stretching sheet includes [6-9].

The involvement of MHD in boundary layer flow is to control the flow of the fluid as it involves the connection between fluid flow and magnetic fields [10]. The MHD viscous flow contributes in process of engineering applications such as cooling of nuclear reactors, modern metallurgical and metal-working. These processes are mainly depending on the application of magnetic field. Mabood *et al.* [11] studied the MHD flow over exponentially stretching sheet using HAM. MHD flow under different physical conditions has been investigated by [12-15].

Manufacturing processes at high temperatures involved radiation and the understanding of radiation heat transfer are important in designing pertinent equipments [16]. The impact of radiation on hydromagnetic boundary layer flow of a viscous incompressible fluid over a stretching sheet has been investigated by Seini and Makinde [17]. Kothandapani and Prakash [18] analyzed the effects of thermal radiation parameter in Williamson nanofluid. Nayak *et al.* [19] studied the influences of radiation in heat and mass transfer effects on boundary layer flow over a stretching sheet.

The homotopy analysis method was developed by Shijun Liao in 1992 that includes some unique concepts such as providing a great freedom to adjust and control the convergence region of solution series [20]. HAM able to provides an analytical approximation solution on numerous nonlinear problems such as nonlinear ordinary differential equations in boundary-layer flow problems, nonlinear fractional differential equations, homogeneous and nonhomogeneous nonlinear differential equations, and higher-order nonlinear differential equations as in [21-25].

The purpose of this present study is to include the heat and mass transfer MHD boundary layer flow over an exponentially stretching sheet with the presence of radiation. Using similarity transformations, the governing partial differential equations are transformed to a system of nonlinear ordinary differential equations. The transformed governing equations are then solved using HAM. HAM will be used to study the flow characteristics of the fluid.

2 Mathematical Formulation

This study considers a steady, two-dimensional MHD flow of viscous incompressible fluid over stretching sheet in the presence of radiation. It is assumed that the surface is stretched with velocity U_w along the x-axis, keeping the origin fixed with the y-axis normal to the x-axis. The sheet with surface temperature T_w and concentration C_w are placed in an inactive fluid of uniform ambient temperature T_∞ and concentration C_∞. A variable magnetic field $B(x) = B_0 e^{x/2L}$ is applied normally to the stretching sheet, where B_0 is a constant. The governing boundary layer equations following [2] and [11] are:

Continuity equation:

$$\frac{\partial u}{\partial x} + \frac{\partial v}{\partial y} = 0, \tag{1}$$

Momentum equation:

$$u\frac{\partial u}{\partial x}+v\frac{\partial u}{\partial y}=\gamma\frac{\partial^2 u}{\partial y^2}-\frac{\sigma B^2}{\rho}u, \tag{2}$$

Energy equation:

$$u\frac{\partial T}{\partial x}+v\frac{\partial T}{\partial y}=\alpha\frac{\partial^2 T}{\partial y^2}-\frac{1}{\rho c_p}\frac{\partial q_r}{\partial y}, \tag{3}$$

Concentration equation:

$$u\frac{\partial C}{\partial x}+v\frac{\partial C}{\partial y}=D\frac{\partial^2 C}{\partial y^2}, \tag{4}$$

where $u$and v are the components of the velocity in the x-, y-directions respectively, γ is the kinematic viscosity, B is magnetic field, α is thermal diffusivity, T is the fluid temperature in the boundary layer, ρ is fluid density, q_r is the radiative heat flux, c_p is the specific heat at constant pressure, C is the concentration in the boundary layer, and D is the molecular diffusivity of chemically reactive species.

According to [17], the Rosseland approximation for radiation in (3) can be written as:

$$q_r=-\frac{4\sigma}{3k^*}\frac{\partial T^4}{\partial y}, \tag{5}$$

where σ is Stefan-Boltzmann constant, and k^* is the absorption coefficient. It is assumed that the temperature difference within the flow is significantly small such that T^4 can be written as a linear function of temperature and after expanding in Taylor series about T_∞ and ignoring higher-order terms resulted in:

$$T^4\approx 4T_\infty^3-3T_\infty^4. \tag{6}$$

Hence, based on (5) and (6), the equation (3) becomes:

$$u\frac{\partial T}{\partial x}+v\frac{\partial T}{\partial y}=\alpha\frac{\partial^2 T}{\partial y^2}+\frac{16\sigma T_\infty^3}{3\rho c_p k^*}\frac{\partial^2 T}{\partial y^2}. \tag{7}$$

The associated boundary conditions for the governing boundary layer equations are:

$$\begin{aligned}&u=U_w(x),\quad v=0,\quad T=T_w=T_\infty+T_0e^{x/2L},\quad C=C_w=C_\infty+C_0e^{x/2L},\ \text{at } y=0,\\ &u\to 0,\quad T\to T_w,\quad C\to C_w,\ \text{as } y\to\infty,\end{aligned} \tag{8}$$

where $U_w(x)=U_0e^{x/L}$ is the stretching velocity, U_0 is the reference velocity, T_w is the variable temperature at the sheet with T_0 being a constant, C_w is the variable concentration on the sheet with C_0 being a constant and L is the characteristic length.

To simplify the mathematical analysis, dimensionless similarity variables are introduced as shown below:

$$\eta=y\sqrt{\frac{U_0}{2\gamma L}}e^{x/2L},\quad u=U_0e^{x/L}f'(\eta),\quad v=-\sqrt{\frac{\gamma U_0}{2L}}e^{x/2L}\left\{f(\eta)+\eta f'(\eta)\right\},$$

$$\theta(\eta)=\frac{T-T_\infty}{T_w-T_0},\quad \phi(\eta)=\frac{C-C_\infty}{C_w-C_0}, \tag{9}$$

where η is the similarity variable, f is the dimensionless stream function, θ is the dimensionless temperature, ϕ is the dimensionless concentration and prime indicates differentiation with respect to η.

Using (9), the nonlinear ordinary differential equations obtained are:

$$f'''(\eta) + f(\eta) f''(\eta) - 2(f'(\eta))^2 - Mf'(\eta) = 0, \tag{10}$$

$$\theta''(\eta)\left(1 + \frac{4}{3}R\right) + \Pr\left(f(\eta)\theta'(\eta) - f'(\eta)\theta(\eta)\right) = 0, \tag{11}$$

$$\phi''(\eta) + Sc\left(f(\eta)\phi'(\eta) - f'(\eta)\phi(\eta)\right) = 0. \tag{12}$$

The new boundary conditions are

$$\begin{aligned} &f(0) = 0, \quad f'(0) = 1, \quad \theta(0) = 1, \quad \phi(0) = 1, \text{ at } \eta = 0, \\ &f'(\infty) \to 0, \quad \theta(\infty) \to 0, \quad \phi(\infty) \to 0, \text{ as } \eta \to \infty \end{aligned} \tag{13}$$

where $M = (2\sigma B_0^2 L)/\rho U_0$ indicates magnetic parameter, $R = (4\sigma T_\infty^3)/k^*\rho c_p \alpha$ is the thermal radiation parameter, $\Pr = \gamma/\alpha$ is the Prandtl number and $Sc = \gamma/D$ indicates the Schmidt number.

The physical quantities involved in this study are local skin-friction coefficient, C_f, local Nusselt number, Nu_x and local Sherwood number, Sh_x which are

$$C_f = \frac{2\tau_w}{\rho U_w^2}, \quad Nu_x = -\frac{xq_w}{T_w - T_\infty}, \quad Sh_x = -\frac{xm_w}{C_w - C_\infty}, \tag{14}$$

where τ_w denoted as the wall shear stress, q_w denoted as the rate of heat transfer and m_w as mass flux, which are given by

$$\tau_w = \mu\left(\frac{\partial u}{\partial y}\right)_{y=0}, \quad q_w = -\left(\frac{\partial T}{\partial y}\right)_{y=0}, \quad m_w = -\left(\frac{\partial C}{\partial y}\right)_{y=0}. \tag{15}$$

Using (9), the local skin-friction coefficient, local Nusselt number and local Sherwood number are

$$f''(0) = \frac{C_f}{\sqrt{\frac{2}{Re_x}\sqrt{\frac{x}{L}}}}, \quad -\theta'(0) = \frac{Nu_x}{\sqrt{\frac{Re_x}{2}\sqrt{\frac{x}{L}}}}, \quad -\phi'(0) = \frac{Sh_x}{\sqrt{\frac{Re_x}{2}\sqrt{\frac{x}{L}}}}, \tag{16}$$

where $Re = (U_w x)/\gamma$ is the local Reynolds number.

3 HAM Solutions

Using HAM, the zeroth-order deformation problems for each dimensionless equation are defined as,

$$(1-q)\,\ell_1\left[f(\eta;q) - f_0(\eta)\right] = q\hbar_f H_1 N_1\left[f(\eta;q)\right], \tag{17}$$

$$(1-q)\,\ell_2\left[\theta(\eta;q) - \theta_0(\eta)\right] = q\hbar_\theta H_2 N_2\left[\theta(\eta;q)\right], \tag{18}$$

$$(1-q)\,\ell_3\left[\phi(\eta;q) - \phi_0(\eta)\right] = q\hbar_\phi H_3 N_3\left[\phi(\eta;q)\right], \tag{19}$$

subject to the boundary conditions based on (13),

$$f\left(0;q\right)=0,\quad f'\left(0;q\right)=1,\quad f'\left(\infty;q\right)=0,\quad \theta\left(0;q\right)=1,\quad \theta\left(\infty;q\right)=0,$$
$$\phi\left(0;q\right)=1,\phi\left(\infty;q\right)=0, \tag{20}$$

The auxiliary linear operators are chosen based on the higher order and lower order of differential equations as in (10) – (12). Then, the auxiliary linear operators are expressed as

$$\ell_1\left(f\right)=\frac{d^3f}{d\eta^3}-\frac{df}{d\eta},\quad \ell_2\left(\theta\right)=\frac{d^2\theta}{d\eta}-\theta,\quad \ell_3\left(\phi\right)=\frac{d^2\phi}{d\eta^2}-\phi, \tag{21}$$

with the following properties,

$$\ell_1\left(C_1+C_2e^{-\eta}+C_3e^{\eta}\right)=0,\quad \ell_2\left(C_4e^{-\eta}+C_5e^{\eta}\right)=0,\quad \ell_3\left(C_6e^{-\eta}+C_7e^{\eta}\right)=0, \tag{22}$$

where $C_i, i=1,2,3,...,7$are arbitrary constants.

From the boundary conditions (13) and according to [11], the initial guesses for (10) – (12) are expressed as follows

$$f_0\left(\eta\right)=1-e^{-\eta},\quad \theta_0\left(\eta\right)=e^{-\eta},\quad \phi_0\left(\eta\right)=e^{-\eta}, \tag{23}$$

The non-linear operator for the zeroth-order deformation equations (17) – (19) are denoted as

$$\begin{aligned}
N_1&=\frac{\partial^3\hat{f}\left(\eta;q\right)}{\partial\eta^3}+\hat{f}\left(\eta;q\right)\frac{\partial^2\hat{f}\left(\eta;q\right)}{\partial\eta^2}-2\left(\frac{\partial\hat{f}\left(\eta;q\right)}{\partial\eta}\right)^2-M\frac{\partial\hat{f}\left(\eta;q\right)}{\partial\eta},\\
N_2&=\left(1+\frac{4}{3}R\right)\frac{\partial^2\hat{\theta}\left(\eta;q\right)}{\partial\eta^2}+\Pr\left(\hat{f}\left(\eta;q\right)\frac{\partial\hat{\theta}\left(\eta;q\right)}{\partial\eta}-\frac{\partial\hat{f}\left(\eta;q\right)}{\partial\eta}\hat{\theta}\left(\eta;q\right)\right),\\
N_3&=\frac{\partial^2\hat{\phi}\left(\eta;q\right)}{\partial\eta^2}+Sc\left(\hat{f}\left(\eta;q\right)\frac{\partial\hat{\phi}\left(\eta;q\right)}{\partial\eta}-\frac{\partial\hat{f}\left(\eta;q\right)}{\partial\eta}\phi\left(\eta;q\right)\right).
\end{aligned} \tag{24}$$

The above non-linear operator, N_1, N_2 and N_3 are taken by referring to ODEs of (10) – (12). From the zeroth-order deformation equations (17) – (19), the $\hbar_f$, $\hbar_\theta$ and $\hbar_\varphi$ represent non-zero auxiliary parameter, H_1, H_2 and H_3 as non-zero auxiliary function where $H_1=H_2=H_3=1$ and the embedding parameter is $q\in[0,1]$.

Thus, the mth-order deformation equations are defined as,

$$\ell_1\left[f_m\left(\eta\right)-\chi_m f_{m-1}\left(\eta\right)\right]=\hbar_f\left(f'''_{m-1}\left(\eta\right)+\sum_{k=0}^{m-1}\left(f_kf''_{m-1-k}-2f'_kf'_{m-1-k}\right)-Mf'_{m-1}\right), \tag{25}$$

$$\ell_2\left[\theta_m\left(\eta\right)-\chi_m\theta_{m-1}\left(\eta\right)\right]=\hbar_\theta\left(\left(1+\frac{4}{3}R\right)\theta''_{m-1}\left(\eta\right)+\Pr\sum_{k=0}^{m-1}\left(f_k\theta'_{m-1-k}-f'_{m-1-k}\theta_k\right)\right), \tag{26}$$

$$\ell_3\left[\phi_m\left(\eta\right)-\chi_m\phi_{m-1}\left(\eta\right)\right]=\hbar_\phi\left(\phi''_{m-1}\left(\eta\right)+Sc\sum_{k=0}^{m-1}\left(f_k\phi'_{m-1-k}-f'_{m-1-k}\phi_k\right)\right), \tag{27}$$

associated with the following boundary conditions,

$$f_m(0) = 0, \quad f'_m(0) = 1, \quad f'_m(\infty) = 0, \quad \theta_m(0) = 1, \quad \theta_m(\infty) = 0,$$
$$\phi_m(0) = 1, \quad \phi_m(\infty) = 0, \tag{28}$$

where

$$\chi_m = \begin{cases} 0, & m \leq 1 \\ 1, & m > 1 \end{cases}.$$

Symbolic software is used to solve the mth-order deformation equations of (25) – (27).

4 Results and Discussion

4.1 Convergence of Homotopy Solution

The $\hbar$-curves determined by plotting the horizontal line segment as shown in Figures 1, 2 and 3. The figures show the HAM solution at 10^{th} order approximation. Figure 1 shows the range of admissible values of $\hbar_f$ for velocity profile is $-1.0 \leq \hbar_f \leq -0.2$. Figure 2 shows the plotted graph with variation values of $\theta'(0)$, against different values of $\hbar_\theta$. The range of admissible values for temperature profile is $-1.5 \leq \hbar_\theta \leq 0.2$ as in Figure 2. Permissible intervals for concentration profiles in Figure 3 are found to be in the range of $-1.9 \leq \hbar_\varphi \leq -0.2$. By HAM, any values from the horizontal line segment will guarantee the convergence of the series. Thus, the value of $\hbar_f = \hbar_\theta = \hbar_\varphi = 0.5$ for velocity, temperature and concentration profiles is used in this work.

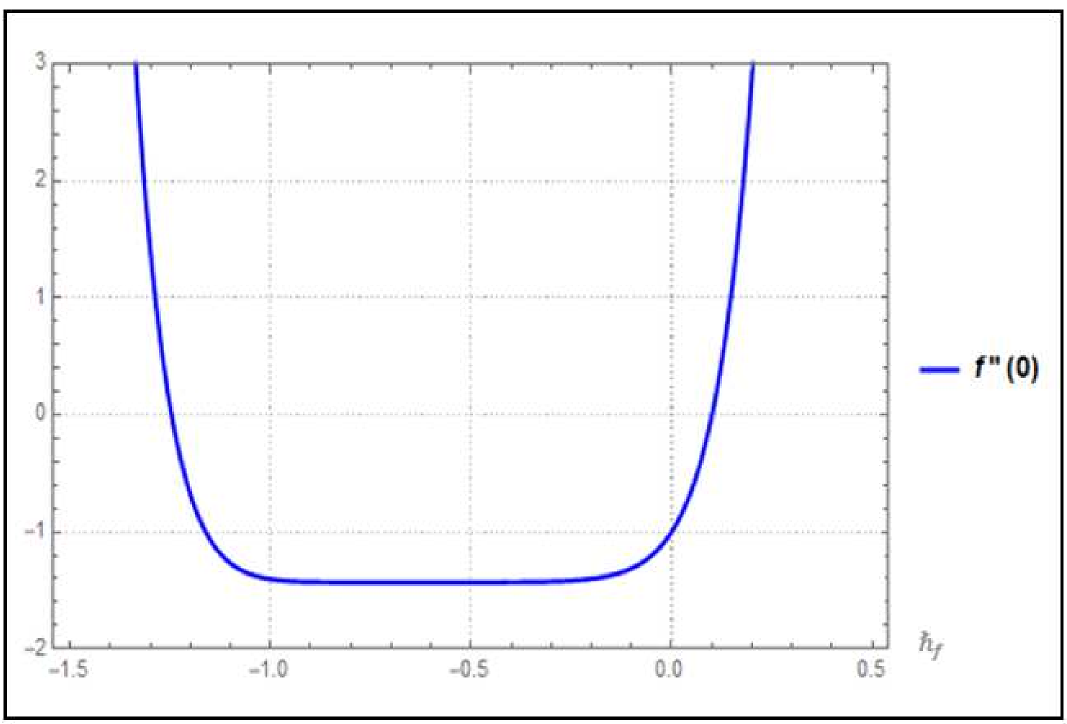

Figure 1: $\hbar$-curve for $f''(0)$

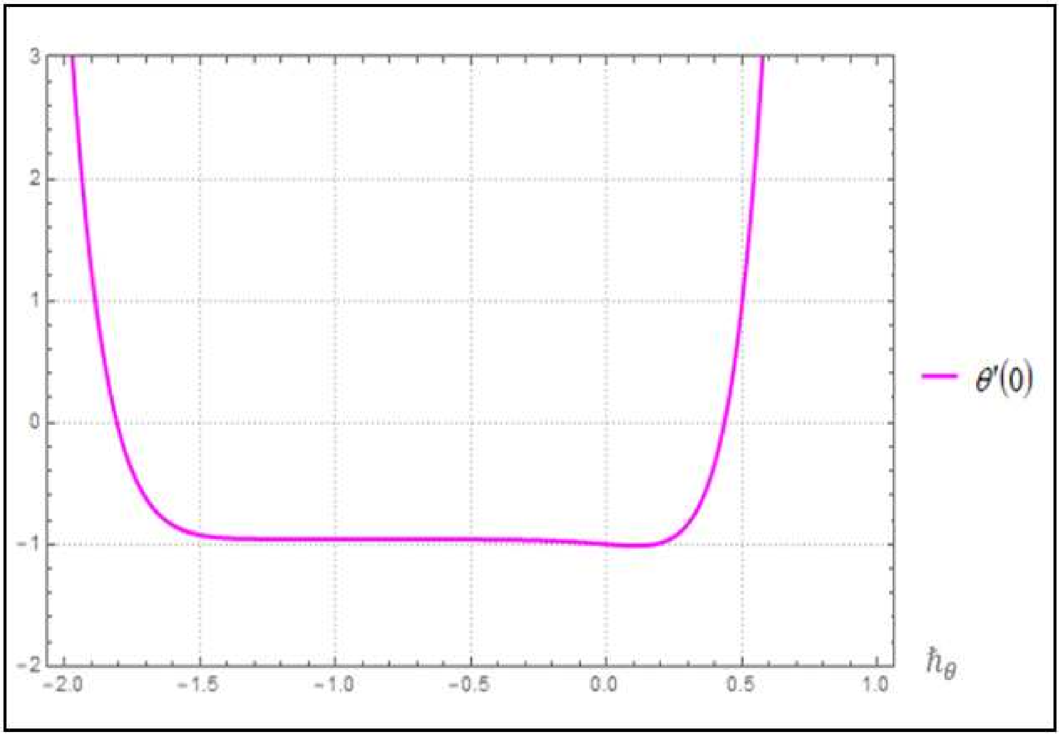

Figure 2: $\hbar$-curve for $\theta'(0)$

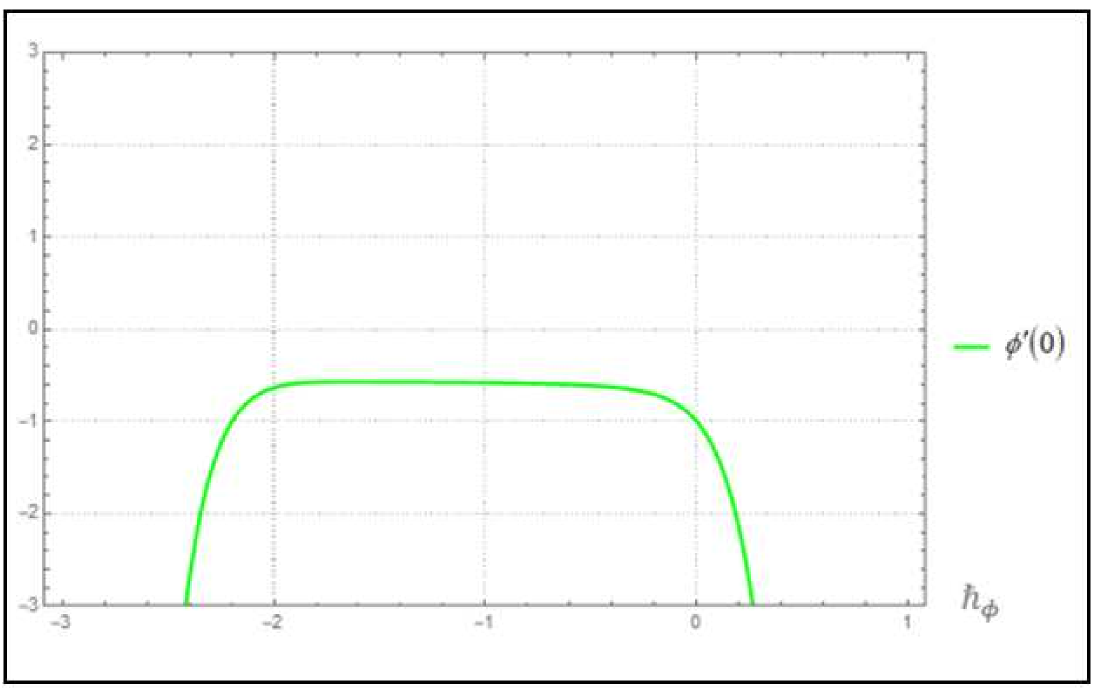

Figure 3: $\hbar$-curve for $\phi'(0)$

4.2 Validation of the Present Study

To ascertain the accuracy and efficiency of homotopy analysis method, a comparison of this study with published data for local Nusselt number, $-\theta'(0)$ is made. Table 1 shows the result obtained from Runge-Kutta method [4] and [18] which is in excellent agreement with the result obtained in this study using HAM.

Table 1: Comparison of Local Nusselt number, $-\theta'(0)$ for Various Values of R, M and Pr with $Sc = 0$

$\boldsymbol{R}$	$\boldsymbol{M}$	**Pr**	**Khalili *et al.* [10]**	**Seini and Makinde [17]**	**Present Study**
0	0	1	0.9550	0.9548	0.9551
		2	1.4714	1.4715	1.4714
		3	1.8690	1.8691	1.8645
0	1	1		0.8615	0.8610

4.3 Results

Figure 4 displays the influence of M parameter on non-dimensional velocity field. The graph shows the increment of magnetic parameter reduces the fluid velocity. Physically, the increasing values of M parameter leads to the existence of Lorentz force where this force has the tendency to produces more resistance to motion of the fluid.

The influence of various values of M and R parameter on dimensionless temperature field are plotted in Figure 5. The graph shows the increment of M increases the temperature distribution. The Lorentz force occurred as the magnetic parameter increases and this causes the temperature to increase and thickens the thermal boundary layer thickness. Figure 5 also shows the dimensionless temperature increases with larger values of R parameter. This occurred due to the augmentation of R parameter improves the changes of energy transport to the surrounding fluid that helps the enhancement in temperature field. Consequently, reduces the rate of heat transfer from the sheet.

Figure 6 represents the effects of various values for Prandtl number and radiation parameter on dimensionless temperature field. The graph displays the increasing values of Prresults in the decrease of thermal diffusivity. In consequence to that, the thermal boundary layer becomes thinner and the heat diffuse away faster from the heated surface. This results in rises of heat capacity which increases the rate of heat transfer.

The effects of magnetic parameter on dimensionless concentration profile is plotted as shown in Figure 7. The graph shows the increasing values of M parameter increases the concentration distribution across boundary layer. Hence, the rate of mass transfer decreases due to the thicker structure of concentration boundary layer. It is noticeable that the features of concentration distribution with increasing values of M are qualitatively equivalent to temperature distribution.

Figure 8 shows the increasing values of Schmidt number reduces the concentration distribution. The increasing values of Sc number indicates the decrease in the particle diffusivity that leads to reduction of the level of concentration. Hence, the concentration boundary layer thickness becomes thinner and results in rises of mass transfer rate. The effect of Schmidt number increases on the concentration boundary layer thickness is analogous to the increasing values of Prandtl number on the thermal boundary layer thickness.

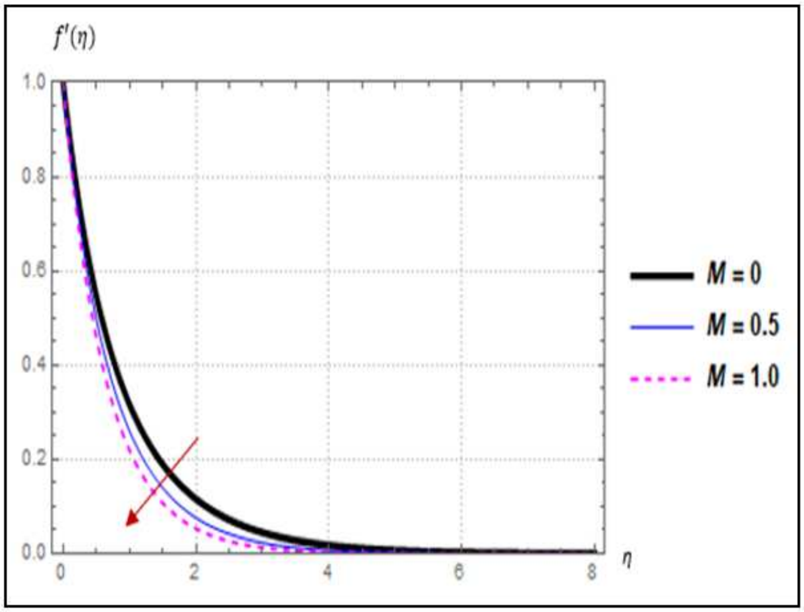

Figure 4: Velocity Profile, $f'(\eta)$ for Different Values of Magnetic Parameter, M with $R = 0.3$, $\Pr = 1.5$, and $Sc = 0.5$

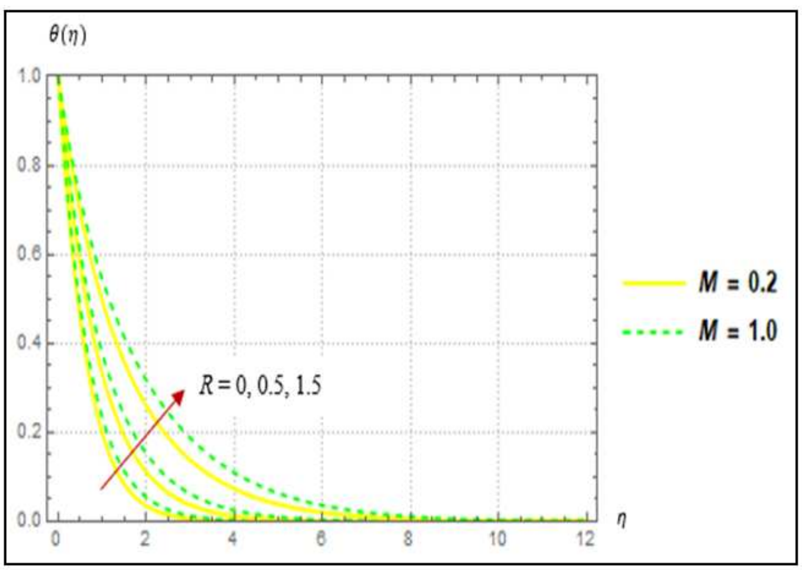

Figure 5: Temperature Profile, $\theta(\eta)$ for Different Values of Magnetic Parameter, M and radiation parameter, R with $\Pr = 2.2$ and $Sc = 0.5$

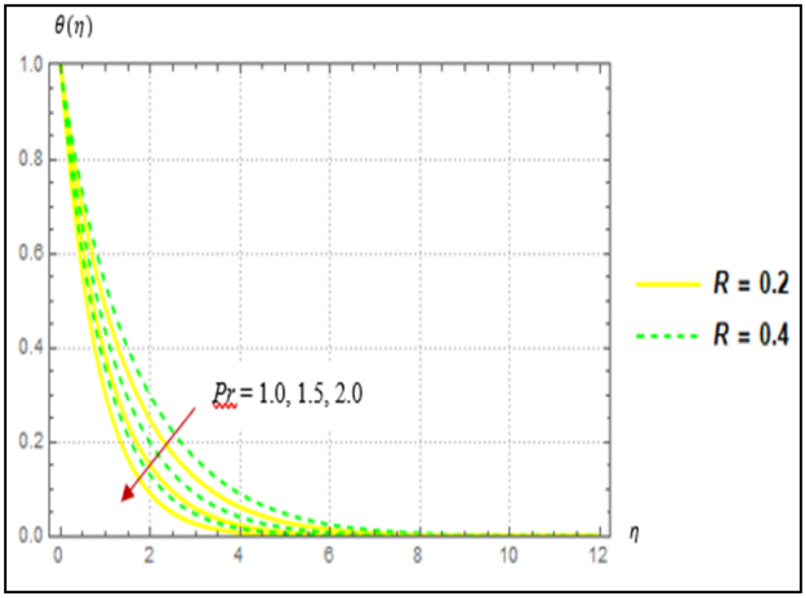

Figure 6: Temperature profile, $\theta(\eta)$ for Different Values of Prandtl number, Pr and radiation parameter, R with $M = 0.5$ and $Sc = 0.5$

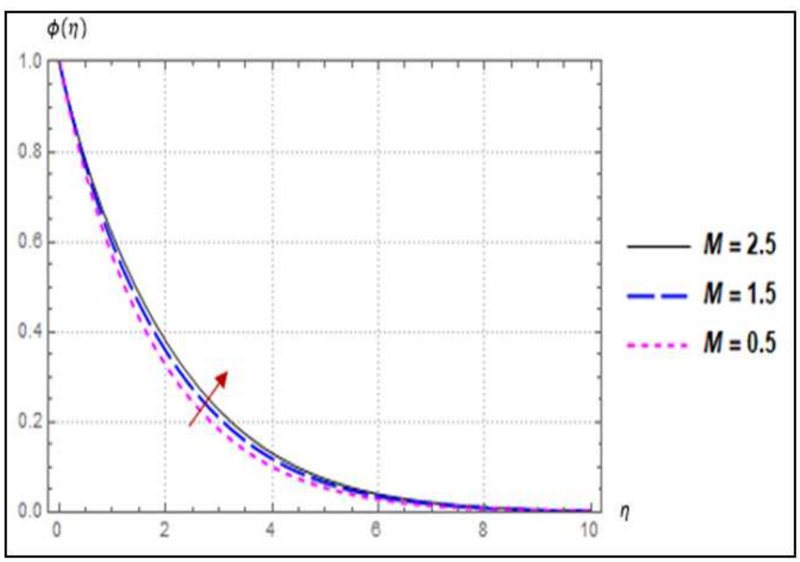

Figure 7: Concentration Profile, $\phi(\eta)$ for Different Values of Magnetic Parameter, M with $Sc = 0.5$

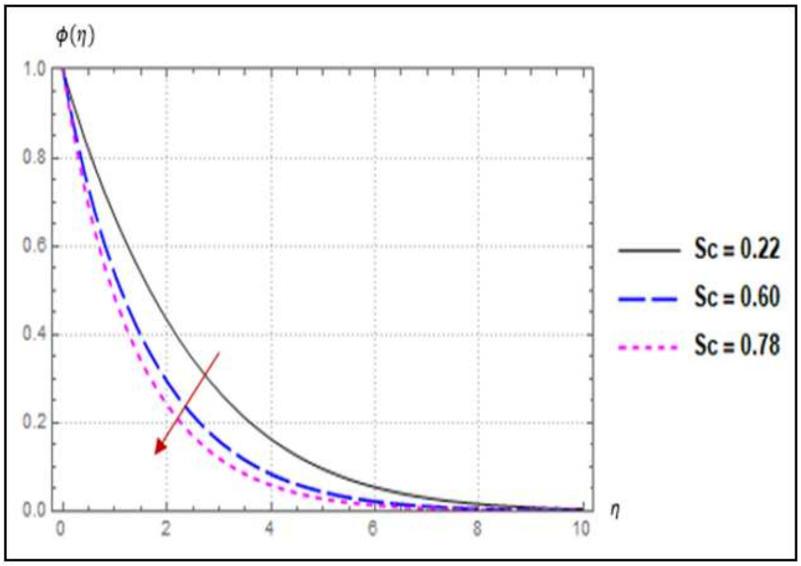

Figure 8: Concentration Profile, $\phi(\eta)$ for Different Values of Schmidt Number, Sc with $M = 0.5$

5 Conclusions

This paper investigated the heat and mass transfer of MHD boundary layer flow of a viscous incompressible fluid over an exponentially stretching sheet in the presence of radiation. The partial differential equations were transformed into nonlinear ordinary differential equations using suitable similarity variables and were solved numerically with HAM method. The results obtained show that increasing the magnetic parameter reduced the velocity but the temperature and concentration of the fluid increased. The temperature increased with higher radiation parameter but decreased as the Prandtl number increased. The concentration distribution of the fluid is reduced with the increasing values of the Schmidt number.

Acknowledgment

The authors would like to acknowledge the financial support received from University Teknologi MARA under the LESTARI Research Grant 600-IRMI/DANA 5/3/LESTARI (0140/2016). The authors wish to thank all the reviewers for their comments and suggestions.

References

[1] Khan, K. A., Butt, A. R., and Raza, N. Effects of heat and mass transfer on unsteady boundary Layer flow of a chemical reacting Casson fluid. *Results in Physics*. 2018. 610-620.

[2] Mohd Fauzi, M. A., Abd Aziz, A. S., and Md Ali, Z. Heat and mass transfer in magnetohydrodynamics (MHD) flow over an exponentially stretching sheet in a thermally stratified medium. *AIP Conference Proceedings*. 1974(1). 2018.

[3] Mori, S., Nakagawa, H., Tanimoto, A., and Sakakibara, M. Heat and mass transfer with a boundary layer flow past a flat plate of finite thickness. *Int. J. Heat Mass Transfer.* 1991. 34(1): 2899-2909.

[4] Sanjayanand, E., and Khan, S. K. On heat and mass transfer in a viscoelastic boundary layer flow over an exponentially stretching sheet. *International Journal of Thermal Sciences*. 2006. 45: 819-828.

[5] Serna, J. Heat and mass transfer mechanisms in nanofluids boundary layers. *International Journal of Heat and Mass Transfer*. 2016. 92: 173-183.

[6] Alinejad, J., and Samarbakhsh, S. Viscous Flow over Nonlinearly Stretching Sheet with Effects of Viscous Dissipation. *Journal of Applied Mathematics.* 2012. 1-10.

[7] Sharma, R., Ishak, A., and Pop, I. Partial slip flow and heat transfer over a stretching sheet in a nanofluid. *Mathematical Problems in Engineering.* 2013.1-7.

[8] Mustafa, M., Khan, J. A., Hayat, T., and Alsaedi, A. Analytical and numerical solutions for axisymmetric flow of nanofluid due to non-linearly stretching sheet. *International Journal of Non-Linear Mechanics.* 2015. 71: 22-29.

[9] Mohd Sohut, N. F., Abd Aziz, A. S., and Md Ali, Z. Double stratification effects on boundary layer flow over a stretching cylinder with chemical reaction and heat generation. *Journal of Physics: Conference Series.* 890. 2017. 1-6. IOP Publishing.

[10] Khalili, N. W., Samson, A. A., Abdul Aziz, A. S., and Ali, Z. M. Chemical reaction and radiation effects on MHD flow past an exponentially stretching sheet with heat sink. *Journal of Physics: Conference Series.* 890. 2017. 1-7.

[11] Mabood, F., Khan, W. A., and Md Ismail, A. I. MHD flow over exponential radiating stretching sheet using homotopy analysis method. *Journal of King Saud University - Engineering Sciences.* 2017. 29: 68-74.

[12] Lok, Y. Y., Ishak, A., and Pop, I. MHD stagnation-point towards a shrinking sheet. *International Journal of Numerical Methods for Heat and Fluid Flow.* 2011. 21(1): 61-72.

[13] Ishak , A. MHD Boundary Layer Flow due to an Exponentially Stretching Sheet with Radiation Effect. *Sains Malaysiana.* 2011. 40(4): 391-395.

[14] Mukhopadhyay, S. MHD Boundary Layer flow and Heat Transfer over an Exponentially Stretching Sheet embedded in a Thermally Stratified Medium. *Alexandria Engineering Journal.* 2013. 52: 259-265.

[15] Zaman, A. S., Abd Aziz, A. S., and Md Ali, Z. Double slip effects of magnetohydrodynamics (MHD) boundary layer flow over an exponentially stretching sheet with radiation, heat source and chemical reaction. *Journal of Physics: Conference Series. 890.* 2017. 1-6. IOP Publishing.

[16] Seddeek, M. A. Effects of radiation and variable viscosity on a MHD free convection flow past a semi-infinite flat plate with an aligned magnetic field in the case of unsteady flow. *International Journal of Heat and Mass Transfer.* 2003. 45: 931-935.

[17] Seini, Y. I., and Makinde, O. D. MHD Boundary Layer Flow due to Exponential Stretching Surface with Radiation and Chemical Reaction. *Mathematical Problems in Engineering.* 2013. 1-7.

[18] Kothandapani, M., and Prakash, J. Effects of thermal radiation parameter and magnetic field on the peristaltic motion of Williamson nanofluids in a tapered asymmetric channel. *International Journal of Heat and Mass Transfer.* 2015. 81: 234-245.

[19] Nayak, M. K., Dash, G. C., and Singh, L. P. Heat and mass transfer effects on MHD viscoelastic fluid over a stretching sheet through porous medium in presence of chemical reaction. *Propulsion and Power Research.* 2016. 5(1): 70-80.

[20] Liao, S. *Homotopy Analysis Method in Nonlinear Differential Equations.* Beijing: Higher Education Press. 2012.

[21] Sajid, M., and Hayat, T. The application of homotopy analysis method for MHD viscous flow due to a shrinking sheet. *Chaos, Solitions and Fractals.* 2009. 39: 1317-1323.

[22] Odibat, Z., Momani, S., and Xu, H. A reliable algorithm of homotopy analysis method for solving nonlinear fractiona differential equations. *Aplied Mathematical Modelling.* 2010. 34: 593-600.

[23] Nazari, M., Salah, F., Aziz, Z. A., and Nilashi, M. Approximate analytic solution for the KdV and Burger Equations with the homotopy analysis method. *Journal of Applied Mathematics.* 2012. 1-13.

[24] David, V. D., Nazari, M., Barati, V., Salah, F., and Aziz, Z. A. Approximate analytical solution for the forced Korteweg-de Vries equation. *Journal of Applied Mathematics.* 2013. 1-9.

[25] Akram, G., and Sadaf, M. Application of homotopy analysis method to the solution of ninth order boundary value problems in AFTI-F16 fighters. *Journal of the Association of Arab Universities for Basic and Applied Sciences.* 2017. 24: 149-155.